Geochronology, 3, 35–47, 2021
https://doi.org/10.5194/gchron-3-35-2021

The use of ASH-15 flowstone as a matrix-matched reference material for laser-ablation U–Pb geochronology of calcite

Perach Nuriel[1], Jörn-Frederik Wotzlaw[2], Maria Ovtcharova[3], Anton Vaks[1], Ciprian Stremtan[4], Martin Šala[5], Nick M. W. Roberts[6], and Andrew R. C. Kylander-Clark[7]

[1]Geological Survey of Israel, 32 Yeshayahu Leibowitz St., Jerusalem, 9692100, Israel
[2]Institute of Geochemistry and Petrology, ETH Zurich, Clausiusstrasse 25, 8092 Zurich, Switzerland
[3]Department of Earth Sciences, University of Geneva, Geneva, Switzerland
[4]Teledyne Photon Machines, 384 Gallatin Park Drive, Bozeman, MT 59715, USA
[5]Department of Analytical Chemistry, National Institute of Chemistry, Hajdrihova 19, 1000 Ljubljana, Slovenia
[6]Geochronology and Tracers Facility, British Geological Survey, Environmental Science Centre, Nottingham, NG12 5GG, UK
[7]Department of Earth Science, University of California, Santa Barbara, CA 93106, USA

Correspondence: Perach Nuriel (nuriel@gsi.gov.il)

Received: 12 July 2020 – Discussion started: 27 July 2020
Revised: 18 November 2020 – Accepted: 19 November 2020 – Published: 14 January 2021

Abstract. Latest advances in laser ablation inductively coupled plasma mass spectrometer (LA-ICPMS) allow for accurate in situ U–Pb dating of carbonate material, with final age uncertainties usually $> 3\,\%$ 2σ. Cross-laboratory reference materials (RMs) used for sample-bracketing are currently limited to WC1 calcite with an age of 254.4 ± 6.5 (2σ). The minimum uncertainty on any age determination with the LA-ICPMS method is therefore $\geq 2.5\,\%$, and validation by secondary RMs is usually performed on in-house standards. This contribution presents a new reference material, ASH-15, a flowstone that is dated here by isotope dilution (ID) thermal ionization mass spectrometry (TIMS) analysis using 37 subsamples, 1–7 mg each. Age results presented here are slightly younger compared to previous ID isotope ratio mass spectrometry (IRMS) U–Pb dates of ASH-15 but within uncertainties and in agreement with in situ analyses using WC1 as the primary RM. We provide new correction parameters to be used as primary or secondary standardization. The suggested $^{238}U/^{206}Pb$ apparent age, not corrected for disequilibrium and without common-lead anchoring, is 2.965 ± 0.011 Ma (uncertainties are 95 % confidence intervals). The new results could improve the propagated uncertainties on the final age with a minimal value of 0.4 %, which is approaching the uncertainty of typical ID analysis on higher-U materials such as zircon. We show that although LA-ICPMS spot analyses of ASH-15 exhibit significant scatter in their isotopic ratios, the down-hole fractionation of ASH-15 is similar to that of other reference materials. This high-U (≈ 1 ppm) and low-Pb (< 0.01 ppm) calcite is most appropriate as a reference material for other speleothem-type carbonates but requires more-sensitive ICP-MS instruments such as the new generation of single-collector and multi-collector ICP-MS. Reference materials with high-Pb and low-U or both low-U and low-Pb compositions are still needed to fully cover the compositional range of carbonate material but may introduce analytical challenges.

1 Introduction

Recent advances in laser ablation techniques applied to multi-phase carbonates allow for accurate dating of a variety of sample types, including calcite cements (Li et al., 2014; Godeau et al., 2018; Anjiang et al., 2019; Holdsworth et al., 2019), hydrothermal veins (Coogan et al., 2016; MacDonald et al., 2019; Piccione et al., 2019), fault-related veins, breccia cement, slickenfibers (Ring and Gerdes, 2016; Roberts and Walker, 2016; Goodfellow et al., 2017; Nuriel et al., 2017, 2019; Hansman et al., 2018; Parrish et al., 2018), and speleothems (Woodhead and Petrus, 2019). With increasing

attention to climatic, seismic, and environmental events in the geological record, there is a growing need for dating techniques that can be accurate and easily implemented for samples at the sub-millimeter scale. This newly emerging technique has the potential to contribute to our understanding of the duration, rate, and extent of these important events in the geological record.

The in situ approach has a great research potential for studying texturally complex samples because it can resolve problems of age mixing of different phases or averaging of continuous growth at the sub-millimeter scale and, thus, increase the overall accuracy of the dated material. While the precision of traditional isotope-dilution (ID) U−Pb analyses is still favorable ($< 1\,\%$ 2σ) (Woodhead and Petrus, 2019), the increasing analytical development of the laser ablation inductively coupled plasma mass spectrometer (LA-ICPMS) method indicates the potential for improving the currently reported uncertainties (usually $> 3\,\%$ 2σ). Finding the right matrix-matched reference material (RM) is a major hurdle for LA analyses of carbonates because of the variety of mineralogy (calcite, dolomite, and aragonite), textures, composition (e.g., high-magnesium calcite, high common lead), and ages (e.g., low radiogenic lead in young samples). Textural differences such as microcrystalline, fine- and coarse-grained material, between the unknown and RMs can contribute to high uncertainties due to differences in ablation efficiency, down-hole fractionation, and differences in crater morphology (e.g., Guillong et al., 2020; Elisha et al., 2020). Observed deviations are potentially up to 20 % of the final intercept age depending on the degree of crater geometry mismatch and are related either to downhole fractionation and/or matrix effects (Guillong et al., 2020).

Currently, the most commonly used procedure for mass-bias correction in the LA method is by standard-sample bracketing. For this, the $^{238}U/^{206}Pb$ LA age of the RMs is corrected to the true RM's $^{238}U/^{206}Pb$ apparent age (not corrected for disequilibrium) as measured independently by an ID isotope ratio mass spectrometry (IRMS) method (thermal ionization mass spectrometry (ID-TIMS) or ID-MC-ICPMS). The RMs are measured throughout each session along with the unknown samples, and a normalization factor is applied to correct both the RMs and the unknowns. Uncertainty propagation onto the age of the unknowns includes the uncertainties of the "true" RM age. As a result, the accuracy of the LA analyses can only be as good as the uncertainties on the age of the RMs, which is by itself subjected to analytical challenges due to natural heterogeneities, impurities, and textural complexities at the sub-millimeter scale. It is therefore essential that the "true age" of the reference material will reflect these complexities while maintaining minimal uncertainties.

Currently, several in-house standards are being used as reference materials, including Duff Brown Tank (64 Ma; Hill et al., 2016), and JT (13.797 ± 0.031 Ma; Guillong et al., 2020). The only well-characterized reference material that is distributed across laboratories is the WC1 calcite with an age of 254.4 ± 6.5 2σ (2.5 %) (Roberts et al., 2017). The use of WC1 alone for mass-bias correction has several disadvantages. First, it is highly recommended with all in situ U−Th−Pb geochronology to use secondary RMs to validate any correction parameters that are being used and to appropriately propagate uncertainties. Second, the relatively high uncertainty (2.5 %) on the age of WC1 sets a minimal uncertainty on any LA U−Pb age determination. Finally, the quantity of the WC1 sample that is currently available for future work is limited and is likely to not fully meet the growing demands of the LA scientific community; however, we note here that there is a potential for further sample collection from the original site.

This contribution introduces a new carbonate reference material that can be widely used for in situ dating of calcite as primary or as cross-reference material with other available standards. We characterize the reference material at various resolutions using a combination of (1) laser ablation imaging (20 µm square beam); (2) LA spot analysis, ≈ 80–110 µm in diameter, conducted on both single-collector and multi-collector (MC) inductively coupled plasma mass spectrometer (ICP-MS); and (3) ID-TIMS analyses of 37 sub-samples (≈ 1–7 mg aliquots). We discuss several key issues related to the use of ASH-15 sample as a RM, including down-hole fractionation, heterogeneities, and previous bulk analyses, to provide the best correction parameters and suggested protocols for users of the LA scientific community.

2 The ASH-15 flowstone

The ASH-15 flowstone was found in Ashalim Cave, a karstic cave in the central Negev Desert (30°56′36.2″ N, 34°44′22.5″ E), southern Israel, which is part of the northern margin of the Saharan–Arabian desert belt. The cave entrance is located at an elevation of 414 m above sea level and 67 km SE from the Mediterranean Sea coast. The cave is a three-dimensional hypogene maze with a total length of 540 m, situated in Turonian limestone rock strata, at depths of 0–31 m below the surface. The cave is richly decorated with vadose speleothems, such as stalagmites, stalactites and flowstone, which are not active today because of the aridity of the climate in the area (Vaks et al., 2010, 2018), but periods of their deposition correspond to past episodes of wet climate in present-day desert. The thickness of the speleothems varies from several centimeters to a few tens of centimeters. The soil above the cave is silicate loess, originating mainly from eolian dust (Crouvi et al., 2010), and the present-day vegetation is composed of sparse xeric shrubs with $< 10\,\%$ vegetation cover.

The vadose speleothems of Ashalim Cave are composed of low-Mg calcite and are divided into a relatively thick Pliocene basal layer and thinner Pleistocene layers above it. The basal layer varies from 5 to 25 cm in thickness and com-

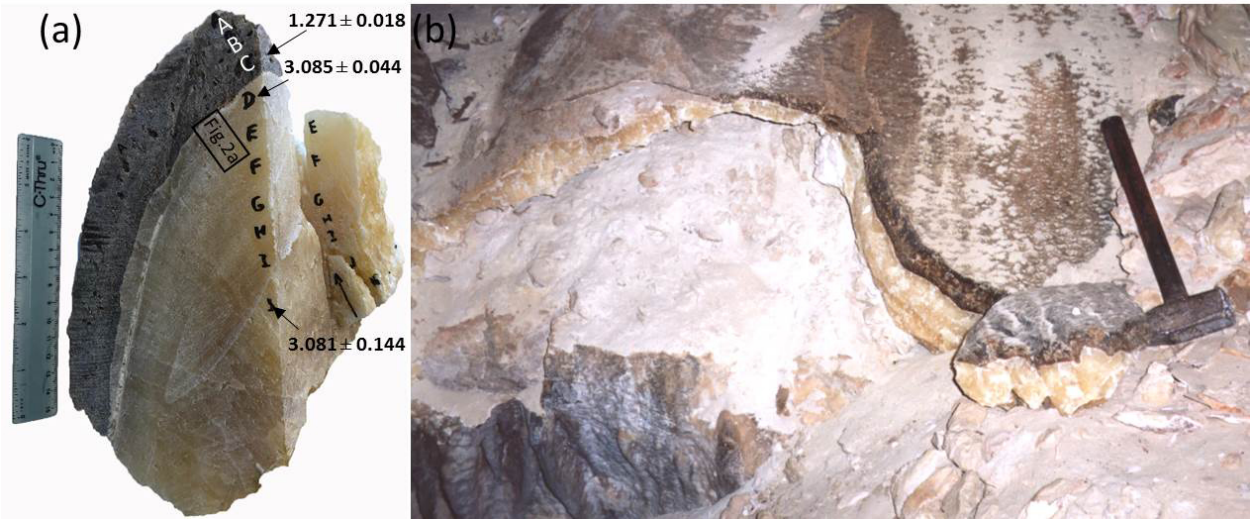

Figure 1. Sample ASH-15 from Ashalim Cave. **(a)** ≈ 5 kg block of sample ASH-15 flowstone consisting of the massive Pliocene yellow basal layer (> 2 cm calcite crystals; section D–K) and the brown Quaternary layer (top section, A–C), the thin layer between the two stratigraphic members represents a growth break (hiatus). The main U−Pb ages of Vaks et al. (2013) are indicated. **(b)** In situ flowstone within Ashalim Cave from which ASH-15 was sampled, showing the large reservoir of this flowstone.

prises ca. 90 % of the speleothem volume in the cave. It is composed of massive yellow calcite crystals (Fig. 1a and b), often showing continuous growth in stalagmites and flowstone, suggesting deposition from continuously dripping water. In all speleothems the basal layer is terminated at its top by a < 1 mm layer of microcrystalline calcite, evaporite minerals, and reddish clays (Fig. 1a), which is interpreted as a hiatus (growth break) separating the basal Pliocene layer and Quaternary layers above it (Vaks et al., 2013). The thickness of Pleistocene top layers varies from several millimeters to 17 cm but usually does not exceed a few centimeters, comprising about 10 % of the speleothem volume in the cave. It is composed of alternating layers of brown calcite, with the youngest top layer (where found) composed of yellow calcite. Several variably colored layers < 1 mm thick of microcrystalline calcite, evaporite minerals, and reddish clays are found within the columnar crystalline structure, suggesting hiatuses in speleothem deposition (Vaks et al., 2013).

The youngest periods of speleothem deposition in several Ashalim Cave speleothems were dated by the ^{238}U−^{230}Th method and occurred from 221 to 190 ka and from 134 to 114 ka (Vaks et al., 2010). Earlier periods of deposition were dated by the U−Pb method on ASH-15 flowstone at 1.272 ± 0.018 Ma (ASH-15-C) and the basal layer of ASH-15 flowstone (layers D–K) at ca. ≈ 3.1 Ma (Fig. 1a). These layers have been dated in three different labs following several protocols for ID analysis (Vaks et al., 2013; Mason et al., 2013). The U concentrations in speleothem calcite range between 1.9 and 19.7 µg g^{-1}, and the amounts of non-radiogenic Th are negligible (Vaks et al., 2010).

2.1 Sample ASH-15 textural characterization

The ASH-15 thin section includes section D and E (see location in Fig. 1a). Overall the thin-section examination indicates that the original texture is preserved with consistent growth direction, no observed hiatus, and no indications for dissolution and recrystallization. A spot analysis array, 85 µm in diameter, targeted along growth zone and along growth direction, is visible in Fig. 2a–c. The ASH-15 sample shows no luminescence under cathodoluminescence light (Fig. 2c), suggesting formation under oxidizing conditions. The slight bright luminescence observed within grain boundaries, discontinuities, and veins (arrows in Fig. 2b and c) may suggest the presence of fluid inclusions, textural differences, or some local replacement within these areas. These areas should be avoided if possible during spot analysis. The relatively homogenous low luminescence may suggest a single-phase continuous calcite growth, whereby precipitation occurred relatively rapidly from the same fluid source (e.g., with consistent Mn^{2+} Fe^{2+} composition) and/or under similar precipitation redox conditions. This 15 cm thick, ≈ 3 Ma Pliocene layer (section D–K) is essentially of the same age. For this reason, previous dating of this sample also considered a similar initial ^{234}U/^{238}U activity ratio for disequilibrium correction (Mason et al., 2013; Vaks et al., 2013). The ASH-15 reference material consists of the whole Pliocene section that terminates with a sharp transition to the darker Pleistocene layers above it (section A–C; see Fig. 1b). About 3 kg of ASH-15 sample is excavated from the Ashalim Cave (Fig. 1a), and potentially much more can be sampled in the future (we estimate more than 10 kg of sample; Fig. 1b). The ASH-15 flowstone is therefore a good candidate for a refer-

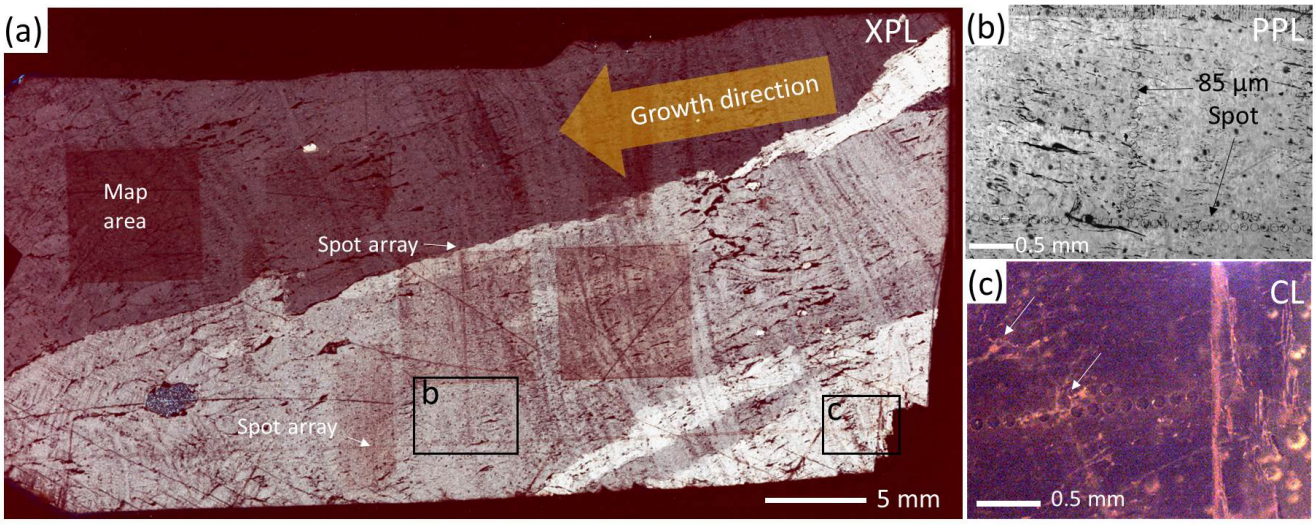

Figure 2. ASH-15D-E thin section. **(a)** Cross-polarized (XPL) scan, 36 mm long, showing continuous growth (no hiatus) and consistent growth direction (indicated with yellow arrow). Spot analyses are targeted either sub-parallel to growth zone or sub-parallel to growth direction; **(b)** close-up of spot array analyses (location is shown in **a**) with 85 µm diameter; **(c)** CL image showing no luminescence except for some bright luminescence within grains boundaries and veins (arrows).

ence material because of its large volume, high U concentrations, and potentially homogenous age, which will be examine next.

3 Methods

3.1 Elemental mapping

The sample ASH-15 was cut perpendicular to the growth zone of section D and E (see Fig. 1b) in order to examine heterogeneities across growth zone and within. Thin sections were then examined under plane- and cross-polarized light (XPL/PPL) and cathodoluminescence (CL) microscopy (Fig. 2). The central part of the thin section was also analyzed for elemental distribution of selected elements. The elemental maps were measured via LA-ICPMS, carried out on a 193 nm ArF excimer laser ablation system (Analyte G2 Teledyne Photon Machines Inc., Bozeman, MT) coupled to an ICP-QMS (Agilent 7900, Agilent Technologies, Santa Clara CA). The laser was equipped with a Photon Machines HelEx II ablation chamber and an Aerosol Rapid Introduction System (ARIS). The experiments were carried out using acquisition parameters (both on the ICP and on the laser) modeled using the approach of van Elteren et al. (2018, 2019) to avoid artifacts (e.g., aliasing, smear, blur). All images (500×500 pixels) were acquired using a 20 µm square beam, fluence of $3.5\,J\,cm^{-2}$, 294 Hz repetition rate and dosage of 10 (10 overlapping pulses per spot size, which amounts to a scanning speed of $588\,\mu m\,s^{-1}$). The masses monitored were ^{88}Sr, ^{137}Ba, ^{206}Pb, ^{208}Pb, ^{232}Th, and ^{238}U, and the images were constructed using the Photon Machines HDIP data reduction software (van Malderen, 2017).

3.2 LA-MC-ICPMS spot analyses

A thin section of ASH-15 was dated by U–Pb laser ablation multi-collector inductively coupled plasma mass spectrometry (LA-MC-ICPMS) following the method described in Nuriel et al. (2017). A Nu Plasma 3D was employed in conjunction with a Photon Machines Excite 193 nm excimer laser equipped with a HelEex two-volume cell. The laser was fired for 15 s during analysis, using a repetition rate of 10 Hz, a spot size of 85 µm, and a fluence of approx. $1\,J\,cm^{-2}$. The Nu Plasma 3D allows for the simultaneous acquisition of ^{238}U, ^{235}U, ^{232}Th, ^{208}Pb, ^{207}Pb, ^{206}Pb, $^{204}Pb(+Hg)$, and ^{202}Hg, where $^{238}U-^{232}Th$ are measured on Faraday detectors and the low-side masses are measured on Daly detectors. Instrumental mass bias was corrected using a two-step approach: both the $^{207}Pb/^{206}Pb$ and $^{206}Pb/^{238}U$ ratios were first corrected to NIST-614 glass reference material in *Iolite 3* using the geochronology reduction scheme (Paton et al., 2010) to account for both mass bias ($^{207}Pb/^{206}Pb$) and instrumental drift ($^{207}Pb/^{206}Pb$ and $^{206}Pb/^{238}U$). The Tera–Wasserburg data, output from *Iolite*, were then plotted, and $^{206}Pb/^{238}U$ ratios of all RMs and unknowns were adjusted such that the primary calcite reference material – WC-1 – yielded an age of 254 Ma (Roberts et al., 2017). This resulted in accurate dates for both our secondary calcite RM: Duff Brown Tank at 66.8 ± 3.4 Ma (previously reported 64 Ma; Hill et al., 2016) and a $^{207}Pb/^{206}Pb$ date of zircon RM at 566.0 ± 2.8 Ma (previously reported 564 Ma; Gehrels et al., 2008). Uncertainty propagation of individual ratios was assessed by reproducibility of the NIST614 and SL RMs ($n = 44$ in both cases) and added in quadrature such that the mean squared weighted deviation (MSWD) of each

weighted average is ≤ 1 and that the uncertainty is no better than 2 % (long-term reproducibility); this resulted in propagated uncertainties of 2.5 % and 2 % for the $^{206}Pb/^{238}U$ and $^{207}Pb/^{206}Pb$ ratios, respectively. Given that the typical uncertainties of the $^{206}Pb/^{238}U$ and $^{207}Pb/^{206}Pb$ ratios of the unknowns were > 10 % and > 3 %, respectively, the uncertainty propagation on individual ratios had little effect on the calculation of the final date of ASH-15. The thin section of ASH-15 was measured both parallel to the length of section (303 spots) and perpendicular to it (101 spots). Data are plotted using Isoplot (Ludwig, 1998).

3.3 LA-ICPMS spot analyses

Analyses were conducted at the Geochronology and Tracers Facility, British Geological Survey (Nottingham, UK). The instrumentation comprised a New Wave Research 193UC excimer laser ablation system fitted with a TV2 cell, coupled to a Nu Instruments Attom single-collector ICP-MS. The method follows the protocols described in Roberts and Walker (2016) and Roberts et al. (2017). Laser parameters varied slightly per session but typically involve a pre-ablation cleaning spot of 150 µm, fired at 10 Hz with a fluence of $\approx 6\,J\,cm^{-2}$ for 2 s, and ablation conditions of 80–100 µm spots, fired at 10 Hz with a fluence of ≈ 6–$8\,J\,cm^{-2}$ for 25–30 s. A 60 s background is taken before every set of standard-bracketed analyses, and a 5 s washout is left between each ablation. Normalization of Pb−Pb ratios is achieved using NIST614 glass (values of Woodhead and Hergt, 2001) and WC-1 carbonate for Pb−U ratios (Roberts et al., 2017). Data reduction uses the time-resolved analysis function of the Nu Instruments Attolab software and an excel spreadsheet, with uncertainty propagation following the recommendations of Horstwood et al. (2016).

3.4 ID-TIMS U−Pb geochronology

ID-TIMS U−Pb geochronology was performed at the Institute of Geochemistry and Petrology of ETH Zurich (ETHZ) and at the Department of Earth Sciences of the University of Geneva (UNIGE). Millimeter-sized chips of the ASH-15-D and ASH-15-K calcite were extracted using stainless-steel tools. Larger chips were further sub-divided, resulting in $\approx$ 1–7 mg aliquots. Individual chips were transferred into 3 mL Savillex beakers and repeatedly ultrasonically cleaned in ultrapure acetone and water. Cleaned sampled were transferred into pre-cleaned 3 mL Savillex beakers, spiked with $\approx$ 5–10 mg EARTHTIME (^{202}Pb-)$^{205}Pb-^{233}U-^{235}U$ tracer solution (Condon et al., 2015) and dissolved in 6 N HCl at 120 °C on a hotplate for $\approx$ 30 min to assure complete dissolution and sample-spike equilibration. Dissolved samples were dried down and redissolved in 1 N HBr. Uranium and Pb were separated using a single-column (50 µL, AG1-X8 resin) HBr−HCl anion exchange chemistry. The Pb fraction was dried down with a drop of H_3PO_4 after a single-column pass. Uranium was dried down, redissolved in 3 N HCl, and further purified with a HCl-based second-column pass before drying it down with a drop of H_3PO_4. Uranium and Pb were loaded on outgassed single Re filaments with ≈ 1 µL of Si-gel emitter for thermal ionization mass spectrometry. Uranium and Pb isotope ratios were measured on a Thermo TRITON Plus at ETHZ and a Thermo TRITON at UNIGE. Lead isotopes were measured on the axial secondary electron multiplier employing dynamic peak-hopping routine collecting masses (202), 204, 205, 206, 207, and 208. Measured Pb isotope ratios were corrected for mass fractionation either using the double spike (ETHZ) or using a mass fractionation factor of 0.15 ± 0.03 % amu^{-1} for single Pb spiked samples (UNIGE). Uranium isotope ratios were measured as uranium oxide (UO_2) employing a static measurement routine with Faraday cups connected to amplifiers with $10^{13}\,\Omega$ feedback resistors (von Quadt et al., 2016; Wotzlaw et al., 2017). Isotope ratios were corrected for isobaric interferences from minor UO_2 isotopologues (Wotzlaw et al., 2017) and for mass fractionation using the double spike assuming a $^{238}U/^{235}U$ ratio of 137.818 ± 0.045 (Hiess et al., 2012) for sample and blank. Total procedural Pb blanks for the HBr-based chemistry at ETHZ are consistently between 0.2 and 0.4 pg. We therefore attribute up to 0.4 pg to laboratory blank with the remaining common Pb being attributed to initial common Pb. Total procedural blanks measured at UNIGE yielded an average of 1.15 pg that was taken as the laboratory blank contribution. Data reduction and uncertainty propagation was performed using Tripoli and an Microsoft Excel-based spreadsheet that uses the algorithms of Schmitz and Schoene (2007). Isochron calculations were performed using IsoplotR (Vermeesch, 2018). All uncertainties are reported at 95 % confidence ignoring systematic uncertainties associated with the tracer calibration and decay constants unless otherwise stated.

4 Results

All analyses were performed on ASH-15-D-K yellow Pliocene layer, abbreviated here as "ASH-15" unless specification of ASH-15-D, E, etc. is indicated. The ASH-15-A-C brown Pleistocene layer is not part of the ASH-15-suggested reference material.

4.1 LA elemental mapping

Elemental mapping for ^{88}Sr, ^{137}Ba, ^{206}Pb, ^{208}Pb, ^{238}U, and $^{238}U/^{206}Pb$ ratio shows that the distribution of most elements is relatively homogeneous (Fig. 3) and in good accordance with the luminescence data. Higher intensities for ^{238}U and ^{88}Sr were observed along grain boundaries and discontinuities, whereas Pb and the rest of the trace elements are more homogeneously distributed, arguing for steady environmental conditions during the deposition. Ten random regions of interest (ROIs) were selected throughout the sample to mimic

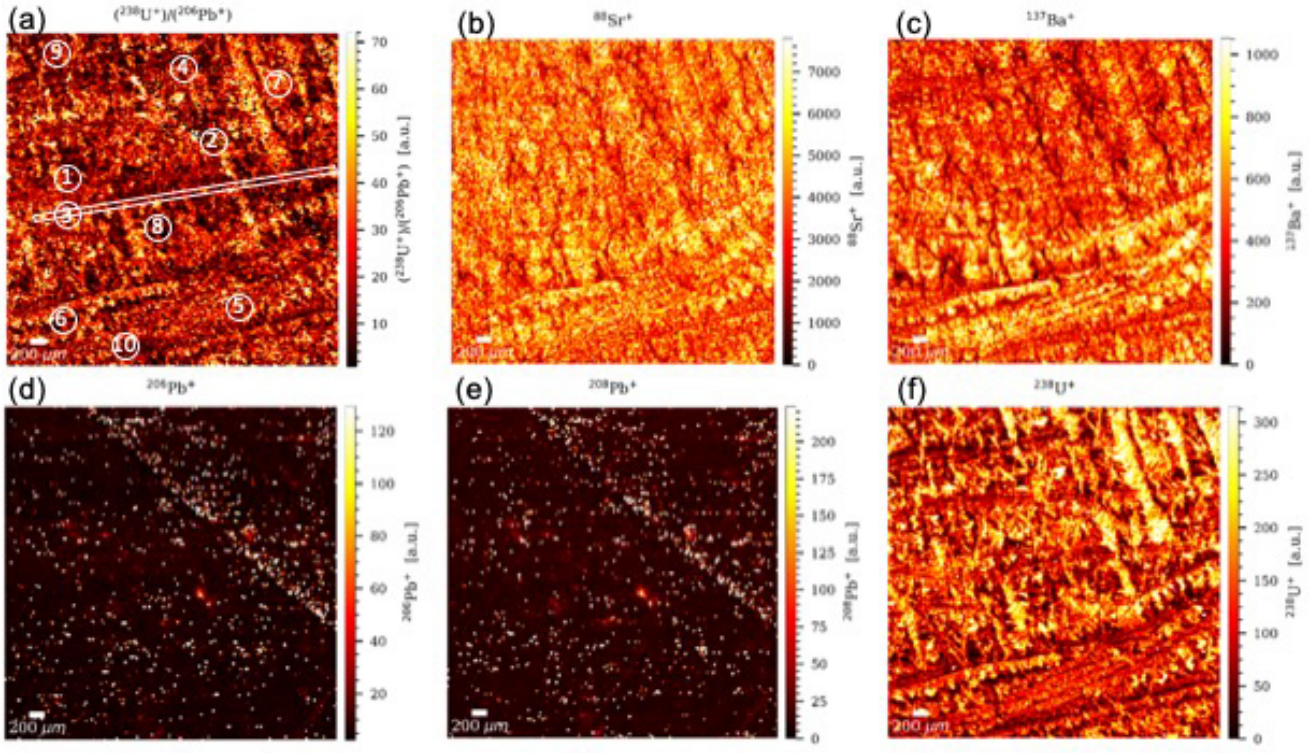

Figure 3. Signal intensity maps of ASH-15. For $^{238}U/^{206}Pb$, ^{88}Sr, ^{137}Ba, ^{206}Pb, ^{208}Pb, and ^{238}U **(a–f)**. The plotted signal was corrected for blank and analytical drift of the instrumentation. Note that each distribution map has its own signal intensity scale. The position of the regions of interest and transect is shown in **(a)**. The circles designating the location of the regions of interest are not to scale (data are available in Table S1).

10 spot analysis carried out at 85–90 µm spot size – just like one would do for U−Pb geochronology. These ROIs were generated by drawing on the map circular regions with the radius of 85 or 90 µm in diameter. The pixels comprising each ROI were pooled together as representing the equivalent of a single spot analysis. The statistical data for each cluster (data are given in the Supplement) were compared. The average values for all pixel data are within 2 standard errors and in good agreement, indicating that, at least based on the elemental distribution we measured, the sample is relatively homogeneous for a natural sample. To further investigate the chemical homogeneity of the sample, a random transect through one of the growth zones was drawn and the signal intensities for ^{238}U were extracted. The transect data also indicate that ^{238}U variations are within 2 standard errors of the average value (full data are available in Table S1 in the Supplement).

4.2 LA-MC-ICPMS spot analyses

Data and calculated ages for the LA-MC-ICPMS transects are shown in Tera–Wasserburg space in Fig. 4 ($n = 379$ of 412 total spots). Analyses rejected from the age calculation include those with $^{207}Pb/^{206}Pb$ uncertainties larger than 0.1 % ($n = 2$) and those with high common-Pb contents (^{208}Pb cps > 5000; $n = 17$). A further 14 spots plotted below the array; these data represent the first 1–2 mm of spots of the lengthwise transect (lower right in Fig. 2a) and suggest that a small percent of ASH-15 may behave differently during ablation and/or may have been subsequently modified after crystallization; upon inspection, this portion of the section contains more pore space and impurities than the majority of the section. The remaining 379 define a normally distributed array with a lower intercept age of 2.952 ± 0.043 Ma (MSWD = 2.5), which is well within uncertainty of the new ID-TIMS data presented (full data are available in Table S2). The calculated upper intercept of each transect is equivalent and within 1 % of the common Pb composition calculated from the ID-TIMS data. Not surprisingly, the lengthwise transect reveals a larger spread in common/radiogenic Pb ratios; this transect crosses more growth zones and has a higher probability of sampling a variety of concentrations of both Pb and U. Conversely, the more limited spread in common/radiogenic Pb ratios appears to reflect the limited sampling of growth zones and would suggest that individual growth zones contain a relatively limited range of concentrations in U and Pb. The slightly higher MSWD for the lengthwise transect (2.7) relative to the growth zone transect (2.5) could also reflect these inherited compositional differ-

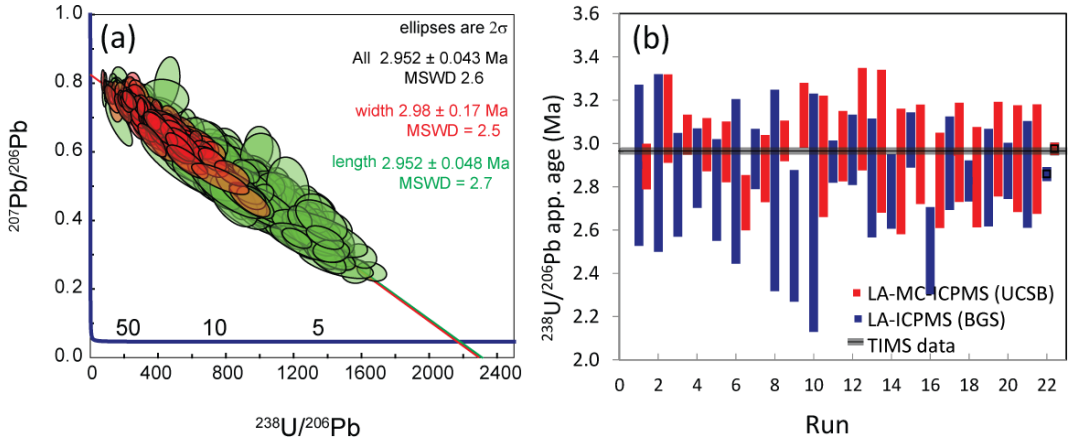

Figure 4. LA-MC-ICPMS analyses of calcite ASH-15. **(a)** Tera–Wasserburg concordia space plot ($n = 385$) for spot analysis within lengthwise transect (green) and along growth zone transect (red). Calculated age, 2σ error, and MSWD are given for both and for all spots together; (full data are available in Table S2); **(b)** variations of ASH-15 ages during different runs using both single-collector (at the British Geological Survey) and multi-collector (at University of California Santa Barbara) ICP-MS. Ages are calculated using WC1 as primary RM; the new ID-TIMS age is indicated with a grey line (full data are available in Tables S3–S5).

ences during growth history and a resulting "mixing" or "averaging" of different growth phases along calcite continuous growth.

Variations of ASH-15 ages during 20 different runs (with 5–30 spot analysis in each) using both single-collector and multi-collector ICP-MS are shown in Fig. 4b (full data are available in Tables S3–S5). The ages are calculated using IsoplotR, not anchored to specific common lead, and are not corrected for disequilibrium. Although there is a large scatter in the ages of the different runs the average ages (marked with black box) plot close to the new ID-TIMS ages or are slightly younger in age.

4.3 Down-hole fractionation

Reference material is important for correction of both laser-induced elemental fractionation (LIEF) and plasma-related ionization efficiency. Ideally, the reference material should resemble the unknown samples as much as possible in terms of its chemistry (e.g., Mg and Fe content), texture (i.e., micritic, crystalline), and age. The WC1 and ASH15 are both low-Mg calcite, but they are very different in textures and age. The ASH15 is a ≈ 3 Ma, well-crystallized elongated calcite (up to 1 cm), and WC1 is a 254 Ma recrystallized botryoidal calcite, formed after aragonite. Despite these differences, both WC1 and ASH15 display a very similar down-hole fractionation pattern (Fig.5d). Figure 5 shows stacked integration plots of the down-hole raw $^{206}Pb/^{238}U$ ratio of different RMs including, the ASH15, WC-1, and Duff Brown Tank (Black and Gulson, 1978). The ASH15 displays much larger scatter in the raw data (Fig. 5a) in comparison to both WC1 and Duff Brown Tank (Fig. 5b and c); however, the average value yielded identical down-hole fractionation to that of WC-1 (Fig. 5d). Duff Brown Tank is also consistent with the down-hole patterns but less steep in comparison to WC1 and ASH15 (Fig. 5d). This comparison suggests that down-hole fractionation and laser-induced elemental fractionation (LIEF) are similar among the different RMs. It is thus suggested that differences in measured and expected $^{206}Pb/^{238}U$ ratios in calcite material are likely to be caused mostly by plasma-ionization differences between unknown samples and RMs.

4.4 ID-TIMS results

Twelve aliquots of ASH-15D analyzed at ETHZ yielded $^{238}U/^{206}Pb$ ratios between 1096 and 2084 and $^{207}Pb/^{206}Pb$ ratios between 0.0825 and 0.4403 (full data are available in Table S6). Plotted in Tera–Wasserburg space, these data yield a single isochron with an initial $^{207}Pb/^{206}Pb$ of 0.832 ± 0.015 (uncertainties are 95 % confidence intervals) and a concordia intercept age of 2.967 ± 0.022 Ma (Fig. 6a). The elevated mean square weighted deviation (MSWD) of 12 is attributed to minor heterogeneities, most likely in the initial $^{207}Pb/^{206}Pb$ ratio of the speleothem calcite. Twelve aliquots of ASH-15K analyzed at ETHZ returned $^{238}U/^{206}Pb$ ratios between 723 and 2094 and $^{207}Pb/^{206}Pb$ ratios between 0.0720 and 0.5677. In Tera–Wasserburg space, 11 out of 12 aliquots define a isochron with an initial $^{207}Pb/^{206}Pb$ of 0.8314 ± 0.0040 and a concordia intercept age of 2.964 ± 0.016 Ma (Fig. 6b). A single aliquot (#5.4) plots significantly below the isochron defined by the other aliquots. The elevated MSWD of 34 together with the single outlier suggests some heterogeneities in the initial $^{207}Pb/^{206}Pb$ of the ASH-15K calcite. Thirteen aliquots of ASH-15K analyzed at UNIGE (pink color, Fig. 6b) yielded $^{238}U/^{206}Pb$ ratios between 433 and 1853 and $^{207}Pb/^{206}Pb$ ratios ranging from 0.1856 to 0.6660. Twelve of the 13 analyses yield a best-

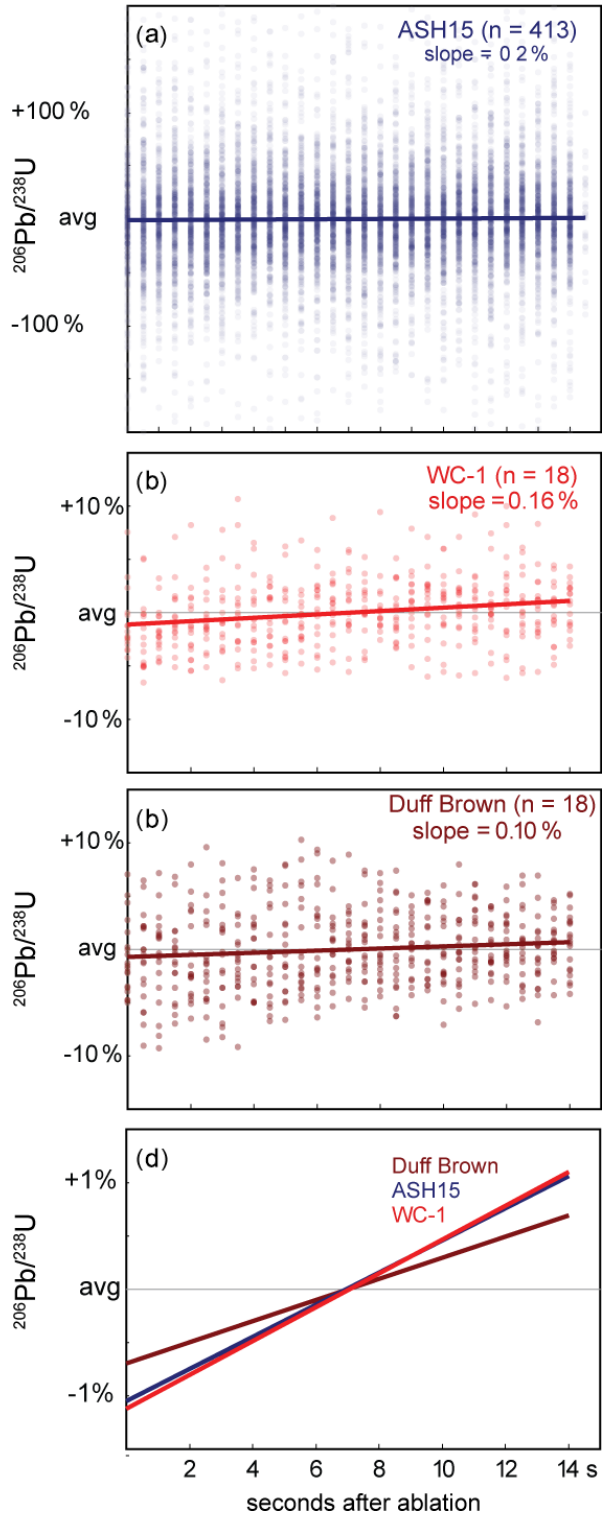

Figure 5. Stacked integration plots of raw ^{207}Pb-corrected ^{206}Pb/^{238}U ratios for calcite reference materials ASH-15, WC-1, and Duff Brown Tank. The low Pb concentration in ASH-15 yields more scatter, but average slopes of all RMs are similar, with 1 %–2 % change in age over 10 s (100 pulses) of ablation. The results suggest minimal differences in down-hole fractionation of the different RMs.

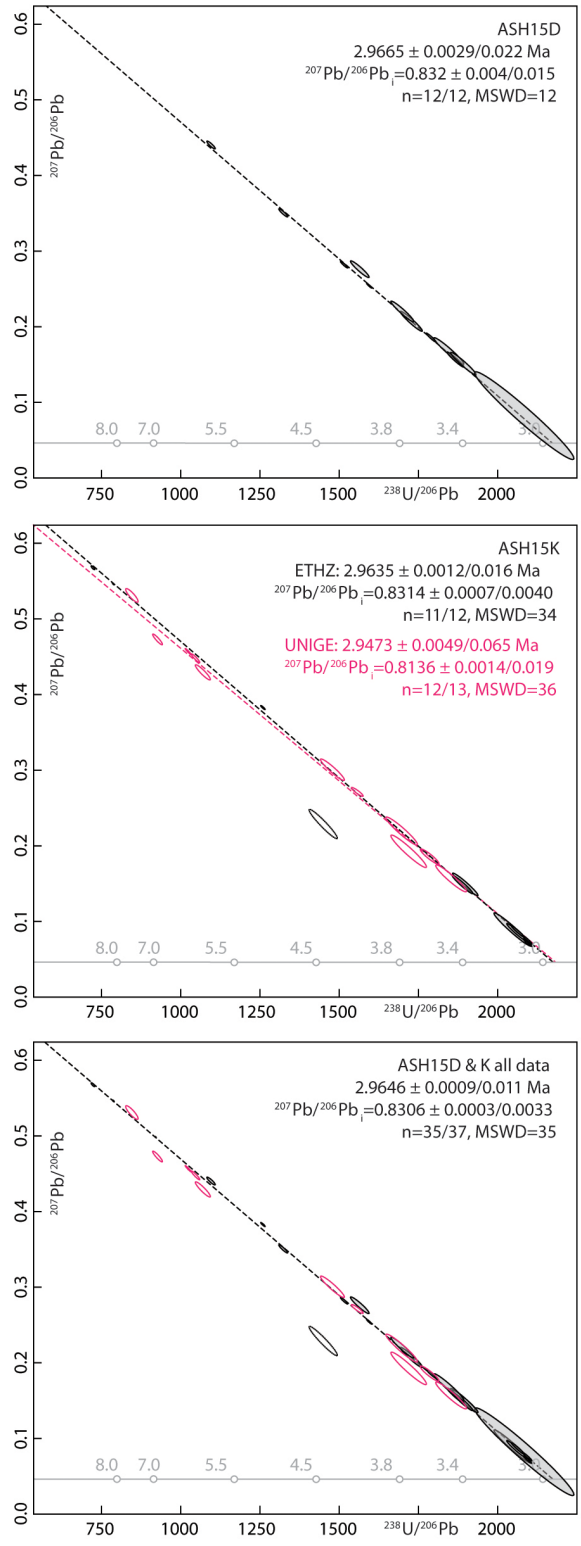

Figure 6. ID-TIMS U–Pb results for ASH-15D, ASH-15K, and for both ASH-15D+K displayed in Tera–Wasserburg concordia space. Uncertainties on the initial ^{207}Pb/^{206}Pb ratios and the intercept ages are reported at 95 % confidence including overdispersion (Vermeesch, 2018).

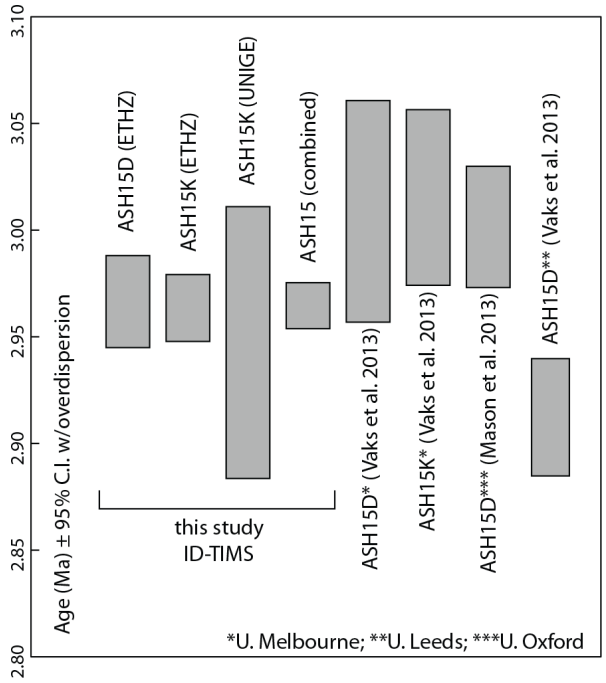

Figure 7. Previous (re-calculated) and new ages of ASH-15 from isotope-dilution U−Pb analysis. All ages are calculated using IsoplotR (Vermeesch, 2018), are not corrected for disequilibrium, and are not anchored to common-lead specific value (see data in Table S7 in the Supplements).

fit line with an initial $^{207}Pb/^{206}Pb$ of 0.814 ± 0.019 and a Concordia intercept age of 2.947 ± 0.065 Ma. The elevated MSWD of 36 confirms the minor heterogeneity of the initial $^{207}Pb/^{206}Pb$.

The excellent agreement between the ASH-15D and ASH-15K datasets indicates that the entire speleothem growth layer between these two growth zones is of equivalent age with minor heterogeneities in the initial $^{207}Pb/^{206}Pb$ ratio and justifies combining the data into a single isochron regression. The combined isochron, using 35 of 37 analyzed aliquots, yields an initial $^{207}Pb/^{206}Pb$ of 0.8306 ± 0.0033 and a concordia intercept age of 2.965 ± 0.011 Ma with a MSWD of 35 (Fig. 6c). We consider the results of the combined regression as the best reference value for using ASH-15 as a primary reference material.

The new TIMS data provide the most extended bulk investigation of the ASH-15 sample, with a total of 37 subsamples that are separated from bottom (K, $n = 25$) to top (D, $n = 12$). The high MSWD of 35 is suggested to reflect true heterogeneities of the dated material, possibly related to impurities that are concentrated within grain boundaries (as suggested by CL and elemental mapping). We re-calculated previously determined isochron ages of Vaks et al. (2013) and Mason et al. (2013; Fig. 7). We obtained concordia intercept ages of 3.0088 ± 0.053 Ma for ASH-15-D (MSWD = 11; $n = 5$) and 3.0153 ± 0.042 Ma for ASH-15-K (MSWD = 14; $n = 5$) of Vaks et al. (2013) and 3.0015 ± 0.029 for ASH-15-D (MSWD = 2; $n = 5$) of Mason et al. (2013). These ages are largely overlapping within uncertainty with our new ID-TIMS age of 2.965 ± 0.011 Ma (Fig. 7; data in Table S7 in the Supplements). The apparent minor systematic offset towards slightly older ages is attributed to the lower number of aliquots in the MC-ICPMS datasets combined with the heterogeneous initial Pb isotope composition. For laser ablation U−Pb work, we recommend the use of the new ID-TIMS age because of the large number of sub-samples ($n = 37$) and the small aliquots (1–7 mg) that are more representative of laser-ablation spot analysis. In addition, the use of the precisely and accurately calibrated EARTHTIME tracer solutions (Condon et al., 2015) and the online mass fractionation correction provided by the double-Pb and double-U tracer are an important advantage of this method. The excellent inter-laboratory reproducibility gives us additional confidence that our ID-TIMS data provide the most accurate characterization of the U−Pb systematics of the ASH-15 calcite for use as a primary reference material.

4.5 Calcite reference material

The U and Pb concentrations of carbonate materials vary greatly. Data compilation by Roberts et al. (2020; this issue) combined hundreds of carbonate samples from different origins such as diagenetic, biogenic, speleothem, and vein fill. This compilation indicates several orders of magnitude differences in U and Pb concentrations of the different types of carbonate and the heterogeneity of spot analysis within each type or even a single sample. A modified representation of their data, excluding calcite vein fill, which vary throughout the entire compositional range, is shown together with the currently available calcite reference materials (Fig. 8; full data in Table S8). Note that both ASH15 and JT display much larger heterogeneity when measured by LA-ICPMS (small symbols) relative to ID-TIMS (large symbols). Despite the high compositional heterogeneity of each of the reference material, they show minimal overlap and together they cover most of the compositional range of the presented carbonate material. WC1 (Roberts et al., 2017) with relatively high U and Pb concentrations can easily be measured on less-sensitive ICP-MS such as quadrupole instruments and is most appropriate to be used for dating vein fill and diagenetic carbonates. In contrast, the ASH15 flowstone, with relatively low Pb and high U concentrations that are better measured on more-sensitive ICP-MS (e.g., new generation of single-collector and multi-collector ICP-MS), is most appropriate for dating speleothem type carbonates. Finally the JT (Guillong et al., 2020), with moderate U and Pb concentration, can be used for most single-collector and multi-collector sector-field ICP-MS instruments as well as the newer generation of quadrupole ICP-MS. Reference material with high Pb and low U or both low U and Pb concentrations will further help

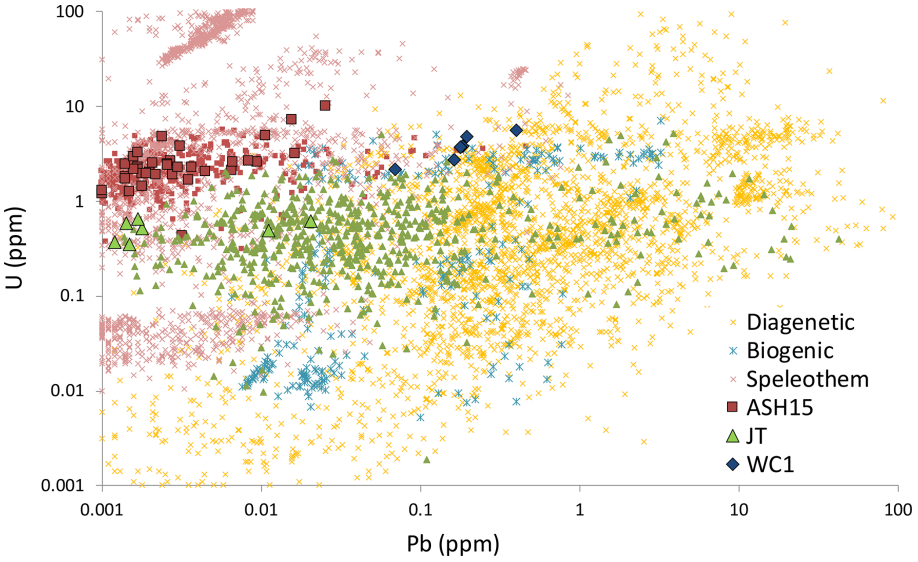

Figure 8. U and Pb concentrations of different carbonate samples and available reference materials. Large and small symbols for the reference materials indicate ID-TIMS and LA-ICPMS analyses, respectively. Note the minimal compositional overlap of the three reference materials (ASH15, WC1, and JT). Data for diagenetic, biogenic, and speleothem carbonates are from Roberts et al. (2020, this issue). Data for JT standard are from Guillong et al. (2020).

to cover the full compositional range of carbonate material but may introduce analytical challenges.

5 Conclusions

The ASH-15 speleothem calcite is characterized as a matrix-matched reference material for LA-ICPMS U−Pb geochronology of calcite. ID-TIMS analyses of small 1–7 mg aliquots of two growth zones suggest sufficient homogeneity with a combined intercept age of 2.965 ± 0.011 Ma and an initial $^{207}Pb/^{206}Pb$ of 0.8315 ± 0.0026. These data are recommended as the reference values for the ASH-15 calcite reference material. The excellent agreement between the two growth zones suggests that the entire interval between the two dated layers can be used with the same reference age. Compared to other calcite reference material (e.g., WC1), ASH-15 is more homogeneous but has lower radiogenic Pb content and therefore requires more sensitive instruments (i.e., sector field rather than quadrupole mass spectrometers) to be used as a reference material.

Appendix A

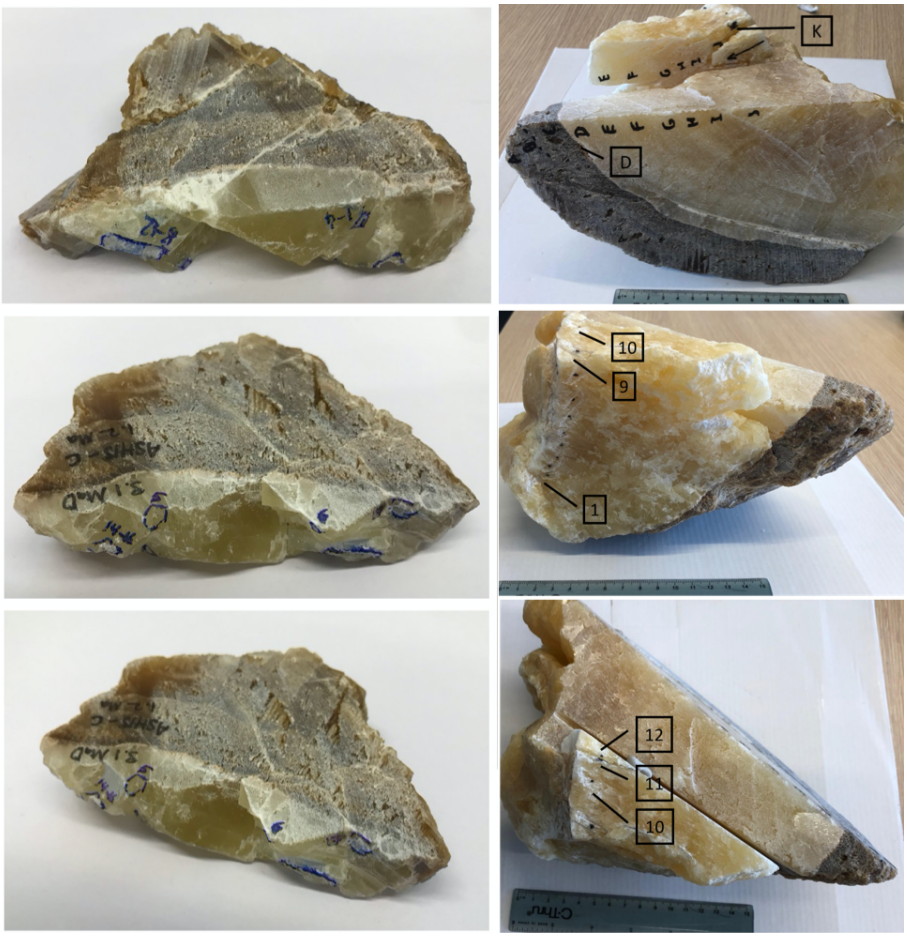

Figure A1. Photographs of ASH15 flowstone with top images showing layers D (light) and A–C (brown) and bottom images showing layers K to D. Sampling localities of aliquots sampled for ID-TIMS analyses are indicated by numbers matching the aliquots in the data Table S6. Larger pieces were chipped off using a stainless-steel needle and subdivided into smaller aliquots for analysis.

Data availability. All data are accessible in the Supplement of the paper.

Supplement. The supplement related to this article is available online at: https://doi.org/10.5194/gchron-3-35-2021-supplement.

Author contributions. PN was responsible for data processing and writing; JFW for ID-TIMS analysis and writing; MO for ID-TIMS analysis; AV for sample collection and writing; CS for LA mapping analysis and writing; MS for LA mapping analysis; NR for LA-ICPMS, data analysis and writing; and AKC for LA-MC-ICPMS, data analysis and writing.

Competing interests. The authors declare that they have no conflict of interest.

Special issue statement. This article is part of the special issue "In situ carbonate U−Pb geochronology". It is a result of the Goldschmidt conference, Barcelona, Spain, 18–23 August 2019.

Acknowledgements. We thank reviewers Fernando Corfu and Jon Woodhead as well as editor, Axel Gerdes, for constructive comments and suggestions. We thank Bar Elisha for thin-section preparation and Andrew Mason for constructive discussion.

Financial support. This research has been supported by the Israel Science Foundation (grant no. ISF-727/16).

Review statement. This paper was edited by Axel Gerdes and reviewed by Jon Woodhead and Fernando Corfu.

References

Anjiang, S., Anping, H., Cheng, T., Liang, F., Wenqing, P., Yuexing, F., and Zhao, J.: Laser ablation in situ U-Pb dating and its application to diagenesis-porosity evolution of carbonate reservoirs, Petroleum Exploration and Development, 46, 1127–1140, 2019.

Black, L. P. and Gulson, B. L.: The age of the Mud Tank carbonatite, Strangways Range, Northern Territory, B.M.R.J. Austral. Geol. Geophys., 3, 227–232, 1978.

Condon, D., Schoene, B., McLean, N., Bowring, S., and Parrish, R.: Metrology and traceability of U–Pb isotope dilution geochronology (EARTHTIME Tracer Calibration Part I), Geoch. Cosmoch. A., 164, 464–480, 2015.

Coogan, L. A., Parrish, R. R., and Roberts, N. M.: Early hydrothermal carbon uptake by the upper oceanic crust: Insight from in situ U-Pb dating, Geology, 44, 147–150, 2016.

Crouvi, O., Amit, R., Enzel, Y., and Gillespie, A. R.: Active sand seas and the formation of desert loess, Quat. Sci. Rev., 29, 2087–2098, 2010.

Elisha, B., Nuriel, P., Kylander-Clark, A., and Weinberger, R.: Towards in-situ U–Pb dating of dolomites, Geochronology Discuss. [preprint], https://doi.org/10.5194/gchron-2020-19, in review, 2020.

Gehrels, G. E., Valencia, V. A., and Ruiz, J. (2008). Enhanced precision, accuracy, efficiency, and spatial resolution of U-Pb ages by laser ablation–multicollector–inductively coupled plasma–mass spectrometry, Geochem. Geophys. Geosyst., 9, Q03017, https://doi.org/10.1029/2007GC001805, 2008.

Godeau, N., Deschamps, P., Guihou, A., Leonide, P., Tendil, A., Gerdes, A., Hamelin, B., and Girard, J.-P. J. G.: U-Pb dating of calcite cement and diagenetic history in microporous carbonate reservoirs: Case of the Urgonian Limestone, France, Geology, 46, 247–250, 2018.

Goodfellow, B. W., Viola, G., Bingen, B., Nuriel, P., and Kylander-Clark, A. R. C.: Palaeocene faulting in SE Sweden from U–Pb dating of slickenfibre calcite, T. Nova, 29, 321–328, https://doi.org/10.1111/ter.12280, 2017.

Guillong, M., Wotzlaw, J.-F., Looser, N., and Laurent, O.: Evaluating the reliability of U–Pb laser ablation inductively coupled plasma mass spectrometry (LA-ICP-MS) carbonate geochronology: matrix issues and a potential calcite validation reference material, Geochronology, 2, 155–167, https://doi.org/10.5194/gchron-2-155-2020, 2020.

Hansman, R. J., Albert, R., Gerdes, A., and Ring, U.: Absolute ages of multiple generations of brittle structures by U-Pb dating of calcite, Geology, 46, 207–210, 2018.

Hiess, J., Condon, D. J., McLean, N., and Noble, S. R.: 238U/235U systematics in terrestrial uranium-bearing minerals, Science, 335, 1610–1614, 2012.

Hill, C. A., Polyak, V. J., Asmerom, Y., and Provencio, P.: Constraints on a Late Cretaceous uplift, denudation, and incision of the Grand Canyon region, southwestern Colorado Plateau, USA, from U-Pb dating of lacustrine limestone, Tectonics, 35, 896–906, 2016.

Hoareau, G., Claverie, F., Pecheyran, C., Paroissin, C., Grignard, P.-A., Motte, G., Chailan, O., and Girard, J.-P.: Direct U-Pb dating of carbonates from micron scale fsLA-ICPMS images using robust regression, Geochronology Discuss. [preprint], https://doi.org/10.5194/gchron-2020-10, in review, 2020.

Holdsworth, R., McCaffrey, K., Dempsey, E., Roberts, N., Hardman, K., Morton, A., Feely, M., Hunt, J., Conway, A., and Robertson, A.: Natural fracture propping and earthquake-induced oil migration in fractured basement reservoirs, Geology, 47, 700–704, 2019.

Horstwood, M. S., Košler, J., Gehrels, G., Jackson, S. E., McLean, N. M., Paton, C., Pearson, N. J., Sircombe, K., Sylvester, P., and Vermeesch, P.: Community-derived standards for LA-ICP-MS U-(Th-) Pb geochronology–Uncertainty propagation, age interpretation and data reporting, Geostand. Geoanal. Res., 40, 311–332, 2016.

Li, Q., Parrish, R., Horstwood, M., and McArthur, J.: U–Pb dating of cements in Mesozoic ammonites, Chem. Geol., 376, 76–83, 2014.

Ludwig, K. R.: Using Isoplot/Ex: Age of Chronological Toolkit for Microsoft Excel, version 1.00, Berkeley Geochronnology Center Special Publication, 1, 1-4, 1998.

MacDonald, J. M., Faithfull, J. W., Roberts, N. M. W., Davies, A. J., Holdsworth, C. M., Newton, M., Williamson, S., Boyce, A., and

John, C. M.: Clumped-isotope palaeothermometry and LA-ICP-MS U–Pb dating of lava-pile hydrothermal calcite veins, Contrib. Mineral. Petr., 174, 63, https://doi.org/10.1007/s00410-019-1599-x, 2019.

Mason, A. J., Henderson, G. M., and Vaks, A.: An Acetic Acid-Based Extraction Protocol for the Recovery of U, Th and Pb from Calcium Carbonates for U-(Th)-Pb Geochronology, Geostand. Geoanal. Res., 37, 261–275, https://doi.org/10.1111/j.1751-908X.2013.00219.x, 2013.

Nuriel, P., Weinberger, R., Kylander-Clark, A. R. C., Hacker, B. R., and Craddock, J. P.: The onset of the Dead Sea transform based on calcite age-strain analyses, Geology, 45, 587–590, https://doi.org/10.1130/g38903.1, 2017.

Nuriel, P., Craddock, J., Kylander-Clark, A. R., Uysal, I. T., Karabacak, V., Dirik, R. K., Hacker, B. R., and Weinberger, R. J. G.: Reactivation history of the North Anatolian fault zone based on calcite age-strain analyses, Geology, 47, 465–469, 2019.

Parrish, R. R., Parrish, C. M., and Lasalle, S.: Vein calcite dating reveals Pyrenean orogen as cause of Paleogene deformation in southern England, J. Geol. Soc., https://doi.org/10.1144/jgs2017-107, 2018.

Paton, C., Woodhead, J. D., Hellstrom, J. C., Hergt, J. M., Greig, A., and Maas, R.: Improved laser ablation U-Pb zircon geochronology through robust downhole fractionation correction. Geochemistry, Geophysics, Geosystems, Geochem. Geophys. Geosyst., 11, Q0AA06, https://doi.org/10.1029/2009GC002618, 2010.

Piccione, G., Rasbury, E. T., Elliott, B. A., Kyle, J. R., Jaret, S. J., Acerbo, A. S., Lanzirotti, A., Northrup, P., Wooton, K., and Parrish, R. R.: Vein fluorite U-Pb dating demonstrates post–6.2 Ma rare-earth element mobilization associated with Rio Grande rifting, Geosphere, 15, 1958–1972, 2019.

Ring, U. and Gerdes, A.: Kinematics of the Alpenrhein-Bodensee graben system in the Central Alps: Oligocene/Miocene transtension due to formation of the Western Alps arc, Tectonics, 35, 1367–1391, 2016.

Roberts, N. M. and Walker, R. J.: U-Pb geochronology of calcite-mineralized faults: Absolute timing of rift-related fault events on the northeast Atlantic margin, Geology, 44, 531–534, 2016.

Roberts, N. M., Rasbury, E. T., Parrish, R. R., Smith, C. J., Horstwood, M. S., and Condon, D. J.: A calcite reference material for LA-ICP-MS U-Pb geochronology, Geochem. Geophy. Geosy., 18, 2807–2814, 2017.

Roberts, N. M. W., Drost, K., Horstwood, M. S. A., Condon, D. J., Chew, D., Drake, H., Milodowski, A. E., McLean, N. M., Smye, A. J., Walker, R. J., Haslam, R., Hodson, K., Imber, J., Beaudoin, N., and Lee, J. K.: Laser ablation inductively coupled plasma mass spectrometry (LA-ICP-MS) U–Pb carbonate geochronology: strategies, progress, and limitations, Geochronology, 2, 33–61, https://doi.org/10.5194/gchron-2-33-2020, 2020.

Schmitz, M. D. and Schoene, B.: Derivation of isotope ratios, errors, and error correlations for U–Pb geochronology using ^{205}Pb–^{235}U–(^{233}U)-spiked isotope dilution thermal ionization mass spectrometric data, Geochem. Geophy. Geosy., 8, Q08006, https://doi.org/10.1029/2006GC001492, 2007.

Vaks, A., Bar-Matthews, M., Matthews, A., Ayalon, A., and Frumkin, A.: Middle-Late Quaternary paleoclimate of northern margins of the Saharan-Arabian Desert: reconstruction from speleothems of Negev Desert, Israel, Quat. Sci. Rev., 29, 2647–2662, 2010.

Vaks, A., Woodhead, J., Bar-Matthews, M., Ayalon, A., Cliff, R. A., Zilberman, T., Matthews, A., and Frumkin, A.: Pliocene–Pleistocene climate of the northern margin of Saharan–Arabian Desert recorded in speleothems from the Negev Desert, Israel, Earth Planet. Sci. Lett., 368, 88–100, https://doi.org/10.1016/j.epsl.2013.02.027, 2013.

Vaks, A., Bar-Matthews, M., Ayalon, A., Matthews, A., and Frumkin, A.: Pliocene–Pleistocene palaeoclimate reconstruction from Ashalim Cave speleothems, Negev Desert, Israel, Geological Society, London, Special Publications, 466, 201–216, 2018.

van Elteren, J. T., Šelih, V. S., Šala, M., Van Malderen, S. J., and Vanhaecke, F.: Imaging artifacts in continuous scanning 2D LA-ICPMS imaging due to nonsynchronization issues, Anal. Chem., 90, 2896–2901, 2018.

van Elteren, J. T., Šelih, V. S., and Šala, M.: Insights into the selection of 2D LA-ICP-MS (multi) elemental mapping conditions, J. Anal. At. Spectr., 34, 1919–1931, 2019.

van Malderen, S.: Optimization of methods based on laser ablation-ICP-mass spectrometry (LA-ICP-MS) for 2-D and 3-D elemental mapping, Doctoral dissertation, Ghent University, Ghent, Belgium, 2017.

Vermeesch, P.: IsoplotR: A free and open toolbox for geochronology, Geosci. Front., 9, 1479–1493, 2018.

von Quadt, A., Wotzlaw, J.-F., Buret, Y., Large, S. J., Peytcheva, I., and Trinquier, A.: High-precision zircon U/Pb geochronology by ID-TIMS using new 10^{13} ohm resistors, J. Anal. At. Spectr., 31, 658–665, 2016.

Woodhead, J. and Petrus, J.: Exploring the advantages and limitations of in situ U–Pb carbonate geochronology using speleothems, Geochronology, 1, 69–84, https://doi.org/10.5194/gchron-1-69-2019, 2019.

Woodhead, J. D. and Hergt, J. M.: Strontium, neodymium and lead isotope analyses of NIST glass certified reference materials: SRM 610, 612, 614, Geol. Newsl., 25, 261–266, 2001.

Wotzlaw, J.-F., Buret, Y., Large, S. J., Szymanowski, D., and von Quadt, A.: ID-TIMS U–Pb geochronology at the 0.1‰ level using 10 13 Ω resistors and simultaneous U and 18 O/16 O isotope ratio determination for accurate UO 2 interference correction, J. Anal. At. Spect., 32, 579–586, 2017.